East Asian Journal on Applied Mathematics
doi: 10.4208/eajam.050818.071018

Vol. **8**, No. 4, pp. 611-633
November 2018

Generalised Müntz Spectral Galerkin Methods for Singularly Perturbed Fractional Differential Equations

Tao Sun[1], Rui-qing Liu[2] and Li-Lian Wang[3,*]

[1]*School of Statistics and Mathematics, Shanghai Lixin University of Accounting and Finance, Shanghai 201209, P. R. China.*
[2]*Institute of Software, Chinese Academy of Sciences, Beijing 100190, and University of Chinese Academy of Sciences, Beijing 100049, P. R. China.*
[3]*Division of Mathematical Sciences, School of Physical and Mathematical Sciences, Nanyang Technological University, 637371, Singapore.*

Received 5 August 2018; Accepted (in revised version) 7 October 2018.

Abstract. A family of orthogonal generalised Müntz-Jacobi functions is introduced and used for solving singularly perturbed fractional differential equations. Such basis functions can provide much better approximation for boundary layers or endpoint singularities than usual polynomial bases. The fractional integrals and derivatives of generalised Müntz-Jacobi functions are accurately calculated. The corresponding Petrov-Galerkin and Galerkin methods are very efficient. Numerical examples demonstrate a significant improvement in the accuracy of the methods.

AMS subject classifications: 65N35, 65E05, 65L11, 26A33, 34A08, 34K26, 41A10

Key words: Mapped Jacobi polynomials, generalised Müntz-Jacobi functions, singularly perturbed fractional differential equations, Petrov-Galerkin methods.

1. Introduction

It is well-known that compared to low-order methods, spectral methods based on global orthogonal polynomials provide a very accurate approximation of smooth solutions with significantly smaller degree of freedom — cf. [4, 9, 21] and references therein. However, they can lose their efficiency if solution exhibits sharp interfaces, strong corner singularities, thin internal and/or boundary layers. In such situations, the usual spectral methods based on Gauss-type grids often fail to produce approximations satisfying the requirements of real physics. A possible solution to this problem would be the use of adaptive method with mesh/grid refinement but the global character of spectral methods does not gracefully handle local mesh refinements. Even for grid adaptation with a moving mesh, the adaptive

*Corresponding author. *Email addresses:* sunt@lixin.edu.cn (T. Sun), ruiqing2017@iscas.ac.cn (R.Q. Liu), lilian@ntu.edu.sg (L.L. Wang)

spectral approximations generated by moving mesh PDEs have to satisfy strong regularity conditions. Therefore, one usually employs a suitable preassigned mapping redistributing the grid points to where they are mostly needed [1,2,12,20]. For example, spectral methods with singular mapping techniques have been successfully used for resolving boundary layers — cf. Refs. [13, 14, 24, 26].

The approach here continues this line. We first show that the application of the singular mapping introduced in [26] to Jacobi polynomials with special parameters, produces mutually orthogonal non-polynomial functions, closely related to the Müntz-Jacobi functions [22] and fractional Jacobi polynomials [10]. The mapped Jacobi polynomials can be now considered as generalised Müntz-Jacobi functions. The present work also focuses on singularly perturbed fractional differential equations, the solutions of which may have sharp boundary layers and corner singularities. One of the main problems here is that the change of variables can lead to more complicated operators and additional singularities. In order to overcome this difficulty, we develop a very accurate scheme to evaluate the results of the action of fractional operators on generalised Müntz-Jacobi functions. Moreover, we consider efficient Petrov-Galerkin methods using special basis functions which can lead to diagonal or symmetric stiffness matrices and to better conditioned linear systems.

The rest of the paper is organised as follows. In Section 2, we introduce mapped Jacobi polynomials, consider their properties and connections with the Müntz-type functions and present an accurate scheme for the evaluation of their fractional integrals and derivatives. The next two sections are devoted to efficient Galerkin methods for singularly perturbed fractional initial value and boundary value problems. In addition, we also consider various examples aimed to show the advantage of the mapping technique proposed.

2. Mapped Jacobi Polynomials and Their Properties

In this section, we introduce mapped Jacobi polynomials and establish accurate formulas for computing the fractional integrals and derivatives of such aggregates. Moreover, we show the close connection of the mapped Jacobi polynomials to the Müntz-type functions. It turns out that the mapped Jacobi polynomials we study, can be considered as generalised Müntz-Jacobi functions. The approximation properties of the mapped Jacobi polynomials are also studied. In particular, we note an improved convergence order for functions with boundary layers and endpoint singularities.

2.1. Singular mappings

Let $\mathbb{N}$ and $\mathbb{R}$ be, respectively, the sets of positive integers and real numbers and let

$$\mathbb{N}_0 := \{0\} \cup \mathbb{N}, \quad \mathbb{R}^+ := \big\{a \in \mathbb{R} : a > 0\big\}, \quad \mathbb{R}_0^+ := \{0\} \cup \mathbb{R}^+. \tag{2.1}$$

Following [26], we consider the one-to-one mapping $g : [-1,1] \to [-1,1]$ defined by

$$x = g(y; r, l) = -1 + \sigma_{r,l} \int_{-1}^{y} (1-t)^r (1+t)^l \, dt, \quad r, l \in \mathbb{N}_0, \tag{2.2}$$

where

$$\sigma_{r,l} = \frac{(r+l+1)!}{2^{r+l}\, r!\, l!}. \tag{2.3}$$

The inverse of this mapping is denoted by

$$y = h(x;r,l) = g^{-1}(x;r,l), \quad x, y \in [-1,1]. \tag{2.4}$$

We note that for $r = 0$ and an integer $l \geq 0$, the mappings (2.2)-(2.4) take the form

$$\begin{aligned} &x = g(y;0,l) = -1 + 2\Big(\frac{1+y}{2}\Big)^{l+1}, \\ &y = h(x;0,l) = -1 + 2\Big(\frac{1+x}{2}\Big)^{1/(l+1)}, \\ &x, y \in [-1,1]. \end{aligned} \tag{2.5}$$

For $r, l \neq 0$, such mappings can redistribute and adapt the grid (collocation) points clustering many of them near the endpoints $x = \pm 1$ — cf. [26]. More precisely, if $\{y_j\}_{j=0}^N$ is a set of Jacobi-Gauss-Lobatto (JGL) points — cf. [21, Chapter 3], arranged in ascending order and $\{x_j = g(y_j;r,l)\}_{j=0}^N$ are the mapped JGL points, then the mean-value theorem yields

$$\begin{aligned} x_j - x_{j-1} &= g(y_j;r,l) - g(y_{j-1};r,l) = g'(\xi_j;r,l)(y_j - y_{j-1}) \\ &= \sigma_{r,l}(1-\xi_j)^r(1+\xi_j)^l(y_j - y_{j-1}), \end{aligned} \tag{2.6}$$

with a $\xi_j \in (y_{j-1}, y_j)$. It follows from [23] that $y_1, y_{N-1} = \mathcal{O}(N^{-2})$ and (2.6) implies

$$1 + x_1 = \mathcal{O}(N^{-2(l+1)}), \quad 1 - x_{N-1} = \mathcal{O}(N^{-2(r+1)}). \tag{2.7}$$

Hence, the sets of the mapped collocation points $\{x_j\}$ in the corresponding half-neighbourhoods of the endpoints $x = \pm 1$ become denser as r, l increase.

Set

$$\tilde{x} := \frac{1 + h(x;r,l)}{2} = \frac{1+y}{2} \in [0,1]. \tag{2.8}$$

In particular, if $r = 0$, then

$$\tilde{x} = \Big(\frac{1+x}{2}\Big)^{1/(l+1)}. \tag{2.9}$$

2.2. Mapped Jacobi polynomials

For $\alpha, \beta > -1$, let $P_{n+1}^{(\alpha,\beta)}(x)$ be the Jacobi polynomials defined by the three-term recurrence relation [23] — viz.

$$\begin{aligned} &P_{n+1}^{(\alpha,\beta)}(x) = (a_n^{\alpha,\beta} x - b_n^{\alpha,\beta}) P_n^{(\alpha,\beta)}(x) - c_n^{\alpha,\beta} P_{n-1}^{(\alpha,\beta)}(x), \quad n \geq 1, \\ &P_0^{(\alpha,\beta)}(x) = 1, \quad P_1^{(\alpha,\beta)}(x) = \frac{1}{2}(\alpha+\beta+2)x + \frac{1}{2}(\alpha-\beta), \end{aligned} \tag{2.10}$$

where

$$a_n^{\alpha,\beta} = \frac{(2n+\alpha+\beta+1)(2n+\alpha+\beta+2)}{2(n+1)(n+\alpha+\beta+1)},$$
$$b_n^{\alpha,\beta} = \frac{(\beta^2-\alpha^2)(2n+\alpha+\beta+1)}{2(n+1)(n+\alpha+\beta+1)(2n+\alpha+\beta)}, \tag{2.11}$$
$$c_n^{\alpha,\beta} = \frac{(n+\alpha)(n+\beta)(2n+\alpha+\beta+2)}{(n+1)(n+\alpha+\beta+1)(2n+\alpha+\beta)}.$$

The Jacobi polynomials are orthogonal with respect to the Jacobi-weight function $\omega^{(\alpha,\beta)}(x) = (1-x)^\alpha(1+x)^\beta$ — i.e.

$$\int_{-1}^{1} P_n^{(\alpha,\beta)}(x)P_{n'}^{(\alpha,\beta)}(x)\omega^{(\alpha,\beta)}(x)\,dx = \gamma_n^{(\alpha,\beta)}\delta_{nn'}, \tag{2.12}$$

where $\delta_{nn'}$ is the Kronecker delta,

$$\gamma_n^{(\alpha,\beta)} = \frac{2^{\alpha+\beta+1}\Gamma(n+\alpha+1)\Gamma(n+\beta+1)}{(2n+\alpha+\beta+1)n!\,\Gamma(n+\alpha+\beta+1)}, \tag{2.13}$$

and Γ refers to the Gamma function. Recall [23] that the derivative of Jacobi polynomials satisfies the following relation:

$$\frac{d}{dx}P_n^{(\alpha,\beta)}(x) = \frac{1}{2}(n+\alpha+\beta+1)P_{n-1}^{(\alpha+1,\beta+1)}(x). \tag{2.14}$$

Definition 2.1. Let $x \in [-1,1]$. The mapped Jacobi polynomials with parameters $r,l \in \mathbb{N}_0$ are defined by

$$\mathscr{L}_n^{(r,l)}(x) = P_n^{(r,l)}(h(x;r,l)) = P_n^{(r,l)}(2\tilde{x}-1) = P_n^{(r,l)}(y), \quad n \geq 0. \tag{2.15}$$

These polynomials can be efficiently evaluated by (2.10)-(2.11).

Let us now present important properties of the mapped Jacobi polynomials.

Proposition 2.1. *The mapped Jacobi polynomials are orthogonal in $L^2(-1,1)$, that is,*

$$\int_{-1}^{1} \mathscr{L}_n^{(r,l)}(x)\mathscr{L}_m^{(r,l)}(x)\,dx = \sigma_{r,l}\gamma_n^{(r,l)}\delta_{mn}, \tag{2.16}$$

where $\sigma_{r,l}$ and $\gamma_n^{(r,l)}$ are defined in (2.3) *and* (2.13).

Proof. Using the orthogonality relation (2.12)-(2.13), we find from (2.2)-(2.3) and (2.15) that

$$\int_{-1}^{1} \mathscr{L}_n^{(r,l)}(x)\mathscr{L}_m^{(r,l)}(x)\,dx = \int_{-1}^{1} P_n^{(r,l)}(y)P_m^{(r,l)}(y)\,\frac{dx}{dy}dy$$
$$= \sigma_{r,l}\int_{-1}^{1} P_n^{(r,l)}(y)P_m^{(r,l)}(y)\,\omega^{(r,l)}(y)\,dy = \sigma_{r,l}\gamma_n^{(r,l)}\delta_{mn},$$

as required. □

Let $\mu \in \mathbb{R}^+$. Following [18], we define the left-sided ${}_{-1}I_x^\mu$ and right-sided ${}_xI_1^\mu$ fractional integrals of order μ on the interval $(-1,1)$ by

$$({}_{-1}I_x^\mu u)(x) = \frac{1}{\Gamma(\mu)} \int_{-1}^{x} \frac{u(y)}{(x-y)^{1-\mu}} dy, \quad ({}_xI_1^\mu u)(x) = \frac{1}{\Gamma(\mu)} \int_{x}^{1} \frac{u(y)}{(y-x)^{1-\mu}} dy. \tag{2.17}$$

If $\mu \in (k-1,k)$, $k \in \mathbb{N}$, then

$$\big({}_{-1}^{C}D_x^\mu u\big)(x) = \big({}_{-1}I_x^{k-\mu} u^{(k)}\big)(x) = \frac{1}{\Gamma(k-\mu)} \int_{-1}^{x} \frac{u^{(k)}(y)}{(x-y)^{\mu-k+1}} dy \tag{2.18}$$

is the left-sided Caputo fractional derivative of order μ. Analogously,

$$\big({}_{x}^{C}D_1^\mu u\big)(x) := (-1)^k ({}_xI_1^{k-\mu} u^{(k)})(x) \tag{2.19}$$

is the right-sided Caputo fractional derivative of order μ.

We observe that the variable change $x = -t$, $t \in (-1,1)$ shows that $({}_tI_1^\mu v)(t) = ({}_{-1}I_x^\mu u)(x)$, where $u(x) = v(-x)$. Similar relations take place for fractional derivatives. Therefore, here we only consider left-sided fractional integrals and derivatives.

Let us now note the following formulas for fractional integrals and derivatives of the mapped Jacobi polynomials.

Theorem 2.1. *If $\mu > 0$ and $r,l \in \mathbb{N}_0$, then*

$${}_{-1}I_x^\mu \mathscr{L}_n^{(r,l)}(x) = \frac{2^{r+l}\sigma_{r,l}}{\Gamma(\mu)} \tilde{x}^{l+1} \int_{-1}^{1} P_n^{(r,l)}(2\tilde{x}\hat{\tau}-1)(1-\tilde{x}\hat{\tau})^r \hat{\tau}^l \{\Phi_{r,l}(x,\tau)\}^{\mu-1} d\tau. \tag{2.20}$$

Moreover, if $\mu \in (0,1)$ and $n \geq 1$, then

$${}_{-1}^{C}D_x^\mu \mathscr{L}_n^{(r,l)}(x) = \frac{n+r+l+1}{2\Gamma(1-\mu)} \tilde{x} \int_{-1}^{1} P_{n-1}^{(r+1,l+1)}(2\tilde{x}\hat{\tau}-1)\{\Phi_{r,l}(x,\tau)\}^{-\mu} d\tau, \tag{2.21}$$

where $\hat{\tau} := (1+\tau)/2$, $\tilde{x}$ is defined in (2.8) *and*

$$\Phi_{r,l}(x,\tau) = 2^{r+l+1}\sigma_{r,l}\, \tilde{x}^{l+1} \int_{\hat{\tau}}^{1} \eta^l (1-\tilde{x}\eta)^r \, d\eta. \tag{2.22}$$

Proof. It follows from (2.15) that

$${}_{-1}I_x^\mu \mathscr{L}_n^{(r,l)}(x) = \frac{1}{\Gamma(\mu)} \int_{-1}^{x} \frac{P_n^{(r,l)}(h(t;r,l))}{(x-t)^{1-\mu}} \, dt. \tag{2.23}$$

Making the variable change

$$t = g\big(-1 + (1+h(x))(1+\tau)/2\big) = g(-1+2\tilde{x}\hat{\tau}), \tag{2.24}$$

with g and h defined in (2.2) and (2.4), we obtain

$$dt = g'(-1+2\tilde{x}\hat{\tau})\tilde{x}d\tau = 2^{r+l}\sigma_{r,l}\,\tilde{x}^{l+1}\hat{\tau}^{l}(1-\tilde{x}\hat{\tau})^{r}\,d\tau, \tag{2.25}$$

and

$$\begin{aligned} x-t &= g(h(x))-g(-1+2\tilde{x}\hat{\tau}) = g(-1+2\tilde{x})-g(-1+2\tilde{x}\hat{\tau}) \\ &= \sigma_{r,l}\int_{-1}^{-1+2\tilde{x}}(1-\xi)^{r}(1+\xi)^{l}d\xi - \sigma_{r,l}\int_{-1}^{-1+2\tilde{x}\hat{\tau}}(1-\xi)^{r}(1+\xi)^{l}d\xi \\ &= \sigma_{r,l}\int_{-1+2\tilde{x}\hat{\tau}}^{-1+2\tilde{x}}(1-\xi)^{r}(1+\xi)^{l}d\xi = 2^{r+l+1}\sigma_{r,l}\,\tilde{x}^{l+1}\int_{\hat{\tau}}^{1}\eta^{l}(1-\tilde{x}\eta)^{r}d\eta \\ &:= \Phi_{r,l}(x,\tau), \end{aligned} \tag{2.26}$$

where $\xi = -1+2\tilde{x}\eta$. Substituting (2.24)-(2.26) into (2.23) yields the Eq. (2.20).

To derive (2.21), we note that according to (2.14)-(2.15), one has

$$\frac{d}{dt}\mathscr{L}_n^{(r,l)}(t) = \frac{1}{2}(n+r+l+1)P_{n-1}^{(r+1,l+1)}\big(h(t)\big)h'(t),$$

and if $\mu \in (0,1)$, then

$${}_{-1}^{C}D_x^{\mu}\,\mathscr{L}_n^{(r,l)}(x) = \frac{n+r+l+1}{2\,\Gamma(1-\mu)}\int_{-1}^{x}P_{n-1}^{(r+1,l+1)}\big(h(t)\big)(x-t)^{-\mu}dh(t).$$

Recalling the Eq. (2.26) and using the relation $dh(t) = \tilde{x}d\tau$, which follows from (2.24), we arrive at the formula (2.21). □

Remark 2.1. If $r = 0$, then

$$\Phi_{0,l}(x,\tau) = 2\tilde{x}^{l+1}(1-\hat{\tau}^{l+1}),$$

and the Eqs. (2.20)-(2.21) take the form

$${}_{-1}I_x^{\mu}\,\mathscr{L}_n^{(0,l)}(x) = \frac{l+1}{\Gamma(\mu)}\frac{(1+x)^{\mu}}{2}\int_{-1}^{1}P_n^{(0,l)}(-1+2\tilde{x}\hat{\tau})\,\hat{\tau}^{l}(1-\hat{\tau}^{l+1})^{\mu-1}\,d\tau, \tag{2.27}$$

$${}_{-1}^{C}D_x^{\mu}\,\mathscr{L}_n^{(0,l)}(x) = \frac{n+l+1}{2^{1+\mu}\Gamma(1-\mu)}\Big(\frac{1+x}{2}\Big)^{1/(l+1)-\mu}\int_{-1}^{1}P_{n-1}^{(1,l+1)}(-1+2\tilde{x}\hat{\tau})(1-\hat{\tau}^{l+1})^{-\mu}d\tau, \tag{2.28}$$

where $\hat{\tau} := (1+\tau)/2$ and $\tilde{x}$ is defined in (2.8).

The case $l = 0$ and $r \neq 0$ can be considered analogously.

2.2.1. Functions $\Phi_{r,l}(x,\tau)$

Since the integrals (2.20)-(2.21) have singular kernels, it is important to study the properties of the functions $\Phi_{r,l}(x,\tau)$. Assume that $r,l>0$ and consider (2.22). Using the mean value theorem, we obtain

$$\begin{aligned}\Phi_{r,l}(x,\tau)&=\frac{2^{r+l+1}\sigma_{r,l}}{r+1}\,\tilde{x}^l\,\eta_0^l\big\{(1-\tilde{x}\hat{\tau})^{r+1}-(1-\tilde{x})^{r+1}\big\}\\&=\frac{2^{r+l+1}\sigma_{r,l}}{r+1}\,\eta_0^l\,\tilde{x}^{l+1}(1-\hat{\tau})\sum_{k=0}^{r}(1-\tilde{x}\hat{\tau})^k(1-\tilde{x})^{r-k},\end{aligned}$$

with an $\eta_0\in(\hat{\tau},1)$. Since $\tilde{x},\hat{\tau}\in(0,1)$, then for all $x,\tau\in(-1,1)$, the inequality

$$\eta_0^l\,\tilde{x}^{l+1}(1-\hat{\tau})(1-\tilde{x})^r\le\frac{\Phi_{r,l}(x,\tau)}{2^{r+l+1}\sigma_{r,l}}\le\eta_0^l\,\tilde{x}^{l+1}(1-\hat{\tau})(1-\tilde{x}\hat{\tau})^r$$

holds. Therefore, $\Phi_{r,l}(x,\tau)\to 0$ as $x,\tau\to 1$. In practical computations, it is often useful to extract the singular factors $(1-t)$ and $(1-x)^r$. However, for arbitrary parameters r,l it can be a time consuming procedure. Let us now consider the case $r=1$ and $l\neq 0$. For simplicity, we introduce the terms

$$S_l(\hat{\tau})=1+\hat{\tau}+\cdots+\hat{\tau}^l,\quad f_l(\hat{\tau})=\frac{S_l(\hat{\tau})}{l+1}=\frac{1+\hat{\tau}+\cdots+\hat{\tau}^l}{l+1}.$$

Since $1-\hat{\tau}^{l+1}=(1-\hat{\tau})S_l(\hat{\tau})$, we can write

$$\int_{\hat{\tau}}^1\eta^l(1-\tilde{x}\eta)d\eta=\int_{\hat{\tau}}^1\eta^l d\eta-\tilde{x}\int_{\hat{\tau}}^1\eta^{l+1}d\eta=(1-\hat{\tau})\Big(\frac{S_l(\hat{\tau})}{l+1}-\tilde{x}\frac{S_{l+1}(\hat{\tau})}{l+2}\Big),$$

and, consequently,

$$\int_{\hat{\tau}}^1\eta^l(1-\tilde{x}\eta)d\eta=(1-\hat{\tau})\,(f_l(\hat{\tau})-\tilde{x}f_{l+1}(\hat{\tau}))\,.$$

For $l=1,2,3$, the terms $f_l(\hat{\tau})$ have the form

$$\begin{aligned}&f_1(\hat{\tau})=1+\frac{1}{2}(\hat{\tau}-1),\quad f_2(\hat{\tau})=1+(\hat{\tau}-1)+\frac{1}{3}(\hat{\tau}-1)^2,\\&f_3(\hat{\tau})=1+\frac{3}{2}(\hat{\tau}-1)+(\hat{\tau}-1)^2+\frac{1}{4}(\hat{\tau}-1)^3,\end{aligned}$$

so that

$$\begin{aligned}&\int_{\hat{\tau}}^1\eta(1-\tilde{x}\eta)d\eta=(1-\hat{\tau})(1-\tilde{x})A_{1,1}(\hat{\tau},\tilde{x}),\\&\int_{\hat{\tau}}^1\eta^2(1-\tilde{x}\eta)d\eta=(1-\hat{\tau})(1-\tilde{x})A_{1,2}(\hat{\tau},\tilde{x}),\\&\int_{\hat{\tau}}^1\eta^3(1-\tilde{x}\eta)d\eta=(1-\hat{\tau})(1-\tilde{x})A_{1,3}(\hat{\tau},\tilde{x}),\end{aligned}$$

where

$$A_{1,1}(\hat{\tau},\tilde{x}) := 1+\frac{(1-\hat{\tau})(\tilde{x}-\frac{1}{2})-\frac{1}{3}(1-\hat{\tau})^2\tilde{x}}{1-\tilde{x}},$$
$$A_{1,2}(\hat{\tau},\tilde{x}) := 1+\frac{(1-\hat{\tau})(\frac{3}{2}\tilde{x}-1)-(1-\hat{\tau})^2(\tilde{x}-\frac{1}{3})+\frac{1}{4}(1-\hat{\tau})^3\tilde{x}}{1-\tilde{x}},$$
$$A_{1,3}(\hat{\tau},\tilde{x}) := 1+\frac{(1-\hat{\tau})(2\tilde{x}-\frac{3}{2})-(1-\hat{\tau})^2(2\tilde{x}-1)+(1-\hat{\tau})^3(\tilde{x}-\frac{1}{4})-\frac{1}{5}(1-\hat{\tau})^4\tilde{x}}{1-\tilde{x}}.$$

Remark 2.2. Using the above representations, we can consider the integrals (2.22) in the most often appearing case $0 \le r,l \le 4$, thus obtaining

$$\Phi_{r,l}(x,\tau) = 2^{r+l+1}\sigma_{r,l}\tilde{x}^{l+1}(1-\hat{\tau})(1-\tilde{x})^r A_{r,l}(\hat{\tau},\tilde{x}). \tag{2.29}$$

2.2.2. Stable and accurate computation of ${}_{-1}I_x^\mu\,\mathscr{L}_n^{(r,l)}(x)$ and ${}_{-1}^{C}D_x^\mu\,\mathscr{L}_n^{(r,l)}(x)$

We now consider fractional integrals and derivatives of the basis functions. Substituting (2.29) into (2.20)-(2.21) leads to the formulas

$$\begin{aligned}
{}_{-1}I_x^\mu\,\mathscr{L}_n^{(r,l)}(x) &= \frac{2^{(r+l+1)\mu-r}\,\sigma_{r,l}^\mu}{\Gamma(\mu)}\,\tilde{x}^{(l+1)\mu}(1-\tilde{x})^{r(\mu-1)}\\
&\quad\times\int_{-1}^{1} P_n^{(r,l)}(2\tilde{x}\hat{\tau}-1)(1-\tilde{x}\hat{\tau})^r\hat{\tau}^l(1-\hat{\tau})^{\mu-1}(A_{r,l}(\hat{\tau},\tilde{x}))^{\mu-1}d\tau,\\
{}_{-1}^{C}D_x^\mu\,\mathscr{L}_n^{(r,l)}(x) &= \frac{n+r+l+1}{2^{1+(r+l+1)\mu}\,\sigma_{r,l}^\mu\Gamma(1-\mu)}\,\tilde{x}^{1-(l+1)\mu}(1-\tilde{x})^{-r\mu}\\
&\quad\times\int_{-1}^{1} P_{n-1}^{(r+1,l+1)}(2\tilde{x}\hat{\tau}-1)(1-\hat{\tau})^{-\mu}(A_{r,l}(\hat{\tau},\tilde{x}))^{-\mu}d\tau.
\end{aligned}\tag{2.30}$$

The explicit extraction of singular fractional powers of $1-\hat{\tau}$ and $1-\tilde{x}$, allows us to use Jacobi-Gauss quadratures. However, if $\tilde{x}\approx 1$ and τ approaches 1, then $(A_{r,l}(\hat{\tau},\tilde{x}))^{\mu-1}$ and $(A_{r,l}(\hat{\tau},\tilde{x}))^{-\mu}$ have boundary layers. This effect is demonstrated in Fig. 1 for parameters $r=1,l=3,\mu=0.1$ and $\tilde{x}=0.99$ for $\tau\in(0.5,1)$. To overcome this problem, we use the variable (2.2) with $r=r_1$, $l=0$ — viz.

$$\tau = g(t;r_1,0) = 1-\frac{(1-t)^{r_1+1}}{2^{r_1}},$$

so that

$$\begin{aligned}
&\int_{-1}^{1} P_n^{(r,l)}(2\tilde{x}\hat{\tau}-1)(1-\tilde{x}\hat{\tau})^r\hat{\tau}^l(1-\hat{\tau})^{\mu-1}(A_{r,l}(\hat{\tau},\tilde{x}))^{\mu-1}d\tau\\
&= (r_1+1)2^{1-(r_1+1)\mu}\int_{-1}^{1} q_n(g(t))\big(A_{r,l}((1+g(t))/2,\tilde{x})\big)^{\mu-1}(1-t)^{(r_1+1)\mu-1}dt,
\end{aligned}\tag{2.31}$$

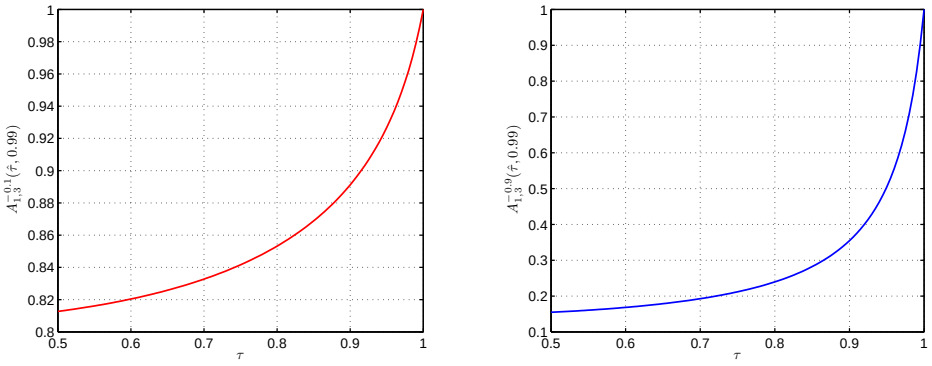

Figure 1: Graphs of $(A_{1,3}(\hat{\tau},0.99))^{-0.1}$ and $(A_{1,3}(\hat{\tau},0.99))^{-0.9}$ for $\tau\in(0.5,1)$.

Table 1: Number of Jacobi-Gauss quadrature points needed to achieve accuracy 10^{-13}.

${}_{-1}I_x^{0.1}\,\mathscr{L}_n^{(3,3)}(x)$						${}_{-1}^{C}D_x^{0.9}\,\mathscr{L}_n^{(3,3)}(x)$					
n \ r_1	1	2	3	4	5	n \ r_1	1	2	3	4	5
50	90	70	80	90	90	50	100	90	160	110	100
100	100	110	130	140	160	100	170	150	160	150	180
150	130	160	180	200	220	150	190	230	220	210	230
200	170	200	230	260	280	200	280	350	230	260	260

where

$$q_n(g(t))=q_n(\tau)=P_n^{(r,l)}(2\tilde{x}\hat{\tau}-1)(1-\tilde{x}\hat{\tau})^r\hat{\tau}^l.$$

Consequently, the integral in (2.31) can be evaluated by the Jacobi-Gauss quadrature with the weight function $\omega^{(\mu r_1+\mu-1,0)}(t)$, since $(r_1+1)\mu-1>\mu-1>-1$. The integral in (2.30) can be considered analogously.

Table 1 shows the number of quadrature points needed to calculate the fractional integrals and derivatives of the mapped Jacobi polynomials with the accuracy 10^{-13}.

2.3. Connections with Müntz-type polynomials/functions

The mapped Jacobi polynomials are closely connected to Müntz-type polynomials and functions — cf. Refs. [3, 7, 10, 15, 17, 22]. In fact, they can be considered as a family of generalised Müntz-Jacobi functions [22].

Let $\Upsilon=\{\lambda_0,\lambda_1,\cdots\}$ be a number sequence such that $0\le\lambda_0<\lambda_1<\cdots\to\infty$. The celebrated Müntz-Szász theorem [5] states that the set of Müntz polynomials $\sum_{k=0}^{n}a_kt^{\lambda_k}$ with real coefficients $\{a_k\}$ is dense in $L^2(0,1)$ if and only if $\sum_{k=1}^{\infty}\lambda_k^{-1}=\infty$. If $\lambda_0=0$, then it is dense in the space $C[0,1]$.

It is of practical interest to study the orthogonal *Müntz-Legendre polynomials*

$$\mathscr{P}_n(t)=\sum_{k=0}^{n}C_{n,k}t^{\lambda_k},\quad C_{n,k}=\frac{\prod_{j=0}^{n-1}(\lambda_k+\lambda_j+1)}{\prod_{k\neq i=0}^{n}(\lambda_k-\lambda_i)},\quad n\geq 0, \tag{2.32}$$

on the interval $[0,1]$. For the properties of the polynomials $\{\mathscr{P}_n\}$, we refer the reader to [3, 15, 17]. Here we only note that these polynomials are orthogonal — i.e.

$$\int_0^1 \mathscr{P}_n(t)\mathscr{P}_m(t)dt=\frac{\delta_{mn}}{\lambda_m+\lambda_n+1}, \tag{2.33}$$

but their evaluation based on the representations (2.32) is extremely unstable.

Nevertheless, if $\lambda_k=k\alpha$ for an $\alpha>0$, the Müntz-Legendre polynomials $\{\mathscr{P}_n\}$ can be explicitly expressed via Jacobi polynomials [7]:

$$\mathscr{P}_n(t)=\mathscr{P}_n(t;\alpha)=P_n^{(0,1/\alpha-1)}(2t^\alpha-1),\quad t\in[0,1],\quad \alpha>0,\quad n\geq 0.$$

Consequently, they can be computed by using the three-term recurrence relations (2.10)-(2.11), whereas the orthogonality relation (2.33) takes the form

$$\int_0^1 \mathscr{P}_n(t)\mathscr{P}_m(t)dt=\frac{\delta_{mn}}{2n\alpha+1}.$$

This type of Müntz polynomials is used in [7] in a collocation method for fractional differential equations.

Setting $y(x)=2^{1-\alpha}(1+x)^\alpha-1$, Shen and Wang [22] rewrote the Müntz polynomials with $\lambda_k=k\alpha$, $\alpha>0$ as the Müntz-Jacobi functions

$$\hat{J}_n^{0,1/\alpha-1}(x)=P_n^{(0,1/\alpha-1)}(y(x)),\quad x,y\in(-1,1),\quad n\geq 0,$$

and used them in Müntz-Galerkin methods [22] for approximation of singular solutions of PDEs with mixed Dirichlet-Neumann boundary conditions. It is worth noting that

$$\hat{J}_n^{0,1/\alpha-1}(x)=\mathscr{P}_n((x+1)/2;\alpha).$$

On the other hand, for $\alpha,\beta>-1$, Hou and Xu [10] introduced the fractional Jacobi polynomials

$$J_n^{\alpha,\beta,\lambda}(t)=P_n^{(\alpha,\beta)}(2t^\lambda-1),\quad \lambda\in(0,1],\quad t\in(0,1),\quad n\geq 0,$$

using them in spectral methods for various singular problems. Let us also note that relations (2.10)-(2.11) yield

$$\int_0^1 J_n^{\alpha,\beta,\lambda}(t)J_m^{\alpha,\beta,\lambda}(t)(1-t^\lambda)^\alpha t^{(\beta+1)\lambda-1}dt=\frac{\gamma_n^{(\alpha,\beta)}}{2^{\alpha+\beta+1}\lambda}\delta_{mn}.$$

If $\alpha=0$ and $\beta=1/\lambda-1$, the fractional Jacobi polynomials become the Müntz-Legendre polynomials, and the variable change $t=(x+1)/2$ transforms them into Müntz-Jacobi functions.

We now discuss the relationship between the mapped Jacobi polynomials in Definition 2.1 and the Müntz-type functions. If $r = 0$, then for any $n, l \in \mathbb{N}_0$, the Eqs. (2.5), (2.8), (2.15) show that

$$\mathscr{L}_n^{(0,l)}(x) = P_n^{(0,l)}(2\tilde{x}-1) = \mathscr{P}_n\big((1+x)/2; 1/(l+1)\big), \quad x \in [-1,1].$$

Thus the mapped Jacobi polynomials turn out to be a special type of Müntz-Legendre polynomials with $\alpha = 1/(l+1)$. Therefore, for $\alpha = 1/(l+1)$ the space

$$\mathscr{M}_N^{(0,l)} = \operatorname{span}\big\{\mathscr{L}_n^{(0,l)}(x) : 0 \le n \le N\big\} = \operatorname{span}\big\{1, (1+x)^{\alpha}, \cdots, (1+x)^{N\alpha}\big\}, \tag{2.34}$$

is dense in $L^2(-1,1)$. For $r, l \neq 0$, the mapped Jacobi polynomials can be considered as generalised Müntz-Jacobi functions

$$\mathscr{M}_N^{(r,l)} = \operatorname{span}\big\{\mathscr{L}_n^{(r,l)}(x) : 0 \le n \le N\big\} = \operatorname{span}\big\{1, \tilde{x}, \cdots, \tilde{x}^N\big\},$$

with $\tilde{x}$ defined in (2.8). Note that to the best of the authors' knowledge, this family of orthogonal functions has not been studied so far.

2.4. Approximation by mapped Jacobi polynomials

Let us now consider the approximation of functions $u \in L^2$ by their orthogonal projections $\pi_N^{(r,l)} u \in \mathscr{M}_N^{(r,l)}$ defined by

$$(\pi_N^{(r,l)}u)(x) = \sum_{n=0}^{N} \hat{u}_n^{(r,l)}\, \mathscr{L}_n^{(r,l)}(x), \quad \hat{u}_n^{(r,l)} = \frac{1}{\sigma_{r,l}\gamma_n^{(r,l)}} \int_{-1}^{1} u(x)\mathscr{L}_n^{(r,l)}(x)\, dx.$$

Using [26], we obtain the following result.

Theorem 2.2. *Let $x = g(y)$ and $y = h(x)$ be, respectively, the mapping* (2.2) *and* (2.4) *and let*

$$\begin{aligned} &\tilde{D}_x u := \frac{dx}{dy}\frac{du}{dx} = \sigma_{r,l}\omega^{(r,l)}(h(x))\frac{du}{dx}, \quad \tilde{D}_x^m u := \underbrace{\tilde{D}_x \cdots \tilde{D}_x}_{m \text{ copies}} u; \\ &\tilde{\omega}_{r,l}^{(\alpha,\beta)}(x) := \omega^{(\alpha,\beta)}(h(x))(g'(h(x); r, l))^{-1}. \end{aligned} \tag{2.35}$$

If $\tilde{D}_x^j u \in L^2_{\tilde{\omega}_{r,l}^{(j+r,j+l)}}(\Lambda)$ for all $0 \le j \le m$, then

$$\|\pi_N^{(r,l)}u - u\| \le cN^{-m}\|\tilde{D}_x^m u\|_{\tilde{\omega}_{r,l}^{(m+r,m+l)}}, \tag{2.36}$$

where the constant c is independent of N and u.

The examples below show how the mapping (2.5) improves the convergence rate.

Example 2.1. Consider the function

$$u(x)=v_0(x)+(1+x)^{\nu_1}v_1(x)+(1+x)^{\nu_2}v_2(x)+\text{h.o.t}, \tag{2.37}$$

where $\{v_i\}$ are smooth functions, $0<\nu_1<\nu_2<\cdots$, and the high-order term contains the singular factor $(1+x)^{\nu}$ with $\nu>\nu_2$. Direct calculations show that if $m<(l+1)(2\nu_1+1)$, then $\|\tilde{D}_x^m u\|_{\tilde{\omega}_{0,l}^{(m,m+l)}}<\infty$. Thus, for the function (2.37), the expected convergence order is $\mathscr{O}(N^{-(l+1)(2\nu_1+1)+\epsilon})$ with a small $\epsilon>0$. For a numerical illustration, we consider the function

$$u(x)=e^x+(1+x)^{\nu_1}\sin x+(1+x)^{\nu_2}\cos x+(1+x)^{\nu_3},$$

with $\nu_1=0.3$, $\nu_2=0.4$ and $\nu_3=1.5$. Computing $|\hat{u}_{N+1}^{(0,l)}|$, we expect that

$$\left\|\pi_N^{(0,l)}u-u\right\|\sim|\hat{u}_{N+1}^{(0,l)}|\sim N^{-(l+1)(2\nu_1+1)+\epsilon}. \tag{2.38}$$

For $l=0,1,2,3$, the desired convergence orders are, respectively, $1.6-\epsilon, 3.2-\epsilon, 4.8-\epsilon$ and $6.4-\epsilon$ with a small $\epsilon>0$, and the left graph in Fig. 2 demonstrates the expected gain in the convergence order.

Example 2.2. Consider now the approximation of the function

$$u_\varepsilon(x)=1-\exp\left(-((1+x)/\varepsilon)^{\nu}\right),\quad \nu\in(0,1),$$

which has a boundary layer due to small ε and the singular factor. Direct calculation shows that

$$\begin{aligned}\tilde{D}_x^m u_\varepsilon=\varepsilon^{-m\nu}(1+x)^{ml/(l+1)+\nu-m}\big\{&c_{m1}\varepsilon^{(m-1)\nu}+c_{m2}\varepsilon^{(m-2)\nu}(1+x)^{\nu}+\cdots\\&+c_{mm-1}\varepsilon^{\nu}(1+x)^{(m-2)\nu}+c_{mm}(1+x)^{(m-1)\nu}\big\}\exp\left(-((1+x)/\varepsilon)^{\nu}\right).\end{aligned}$$

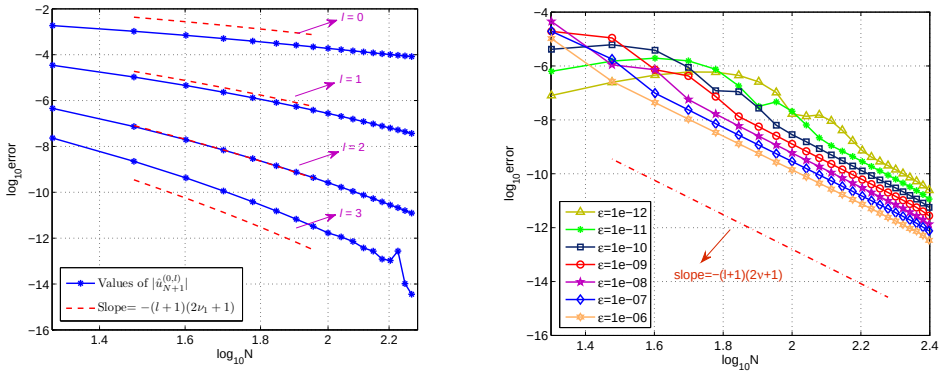

Figure 2: The approximation errors measured by (2.38) and (2.41). Left: Example 2.1. Right: Example 2.2.

Here, $\{c_{mk}\}_{k=1}^{m}$ are constants, which are not in powers of $1/\varepsilon^{\nu}$. It follows from (2.35)-(2.36) that

$$\begin{aligned}\|\tilde{D}_x^m u_\varepsilon\|^2_{\tilde{\omega}^{(m,m+l)}_{0,l}} &\le C\int_{-1}^{1}(\tilde{D}_x^m u_\varepsilon)^2(1+x)^{\frac{m}{l+1}}dx\\ &\le C\sum_{j=1}^{m}\varepsilon^{-2j\nu}\int_{-1}^{1}(1+x)^{2j\nu-\frac{m}{l+1}}\exp\big(-2((1+x)/\varepsilon)^{\nu}\big)dx. \end{aligned}\tag{2.39}$$

Note that if $\alpha>-1$, then the variable change $t=2((1+x)/\varepsilon)^{\nu}$ in the integral below shows that

$$\begin{aligned}&\int_{-1}^{1}(1+x)^{\alpha}\exp\big(-2((1+x)/\varepsilon)^{\nu}\big)dx\\ &=\frac{1}{\nu}\left(\frac{1}{2}\right)^{\frac{\alpha+1}{\nu}}\varepsilon^{\alpha+1}\int_0^{2(\frac{2}{\varepsilon})^{\nu}}t^{\frac{\alpha+1}{\nu}-1}e^{-t}\,dt\le\frac{1}{\nu}\left(\frac{1}{2}\right)^{\frac{\alpha+1}{\nu}}\varepsilon^{\alpha+1}\int_0^{\infty}t^{\frac{\alpha+1}{\nu}-1}e^{-t}\,dt\\ &=\frac{1}{\nu}\left(\frac{1}{2}\right)^{\frac{\alpha+1}{\nu}}\varepsilon^{\alpha+1}\Gamma\left(\frac{\alpha+1}{\nu}\right).\end{aligned}\tag{2.40}$$

If $2\nu-m/(l+1)>-1$, we can set $\alpha=2j\nu-m/(l+1)$ in (2.39)-(2.40) and obtain

$$\|\tilde{D}_x^m u_\varepsilon\|_{\tilde{\omega}^{(m,m+l)}_{0,l}}\le C\varepsilon^{(1-m/(l+1))/2},$$

where C is a constant independent of ε. Therefore, it follows from (2.36) that

$$\|\pi_N^{(0,l)}u_\varepsilon-u_\varepsilon\|\le CN^{-m}\varepsilon^{(1-m/(l+1))/2},\quad m<(l+1)(2\nu+1).\tag{2.41}$$

The convergence order is roughly $\mathcal{O}(\varepsilon^{-\nu}N^{-(l+1)(2\nu+1)+\epsilon})$ for an $0<\epsilon<1$. For numerical illustration, we choose $\nu=0.3, l=3$. The right graph in Fig. 2 shows $|\hat{u}^{(0,l)}_{\varepsilon,N+1}|$ against $N^{-(l+1)(2\nu+1)}$ in $\log_{10}$-scale with $N\in[20,250]$ for various ε. The expected gain in convergence order is visible even for very small ε and thin boundary layer.

3. Applications to Singularly Perturbed FIVPs

We now apply the mapped Jacobi polynomials to singularly perturbed Caputo FIVPs of order $\nu\in(0,1)$.

3.1. Singularly perturbed FIVPs

Let us start with the following singularly perturbed Caputo FIVP of order $\nu\in(0,1)$:

$$\begin{aligned}&\varepsilon\ {}^{C}_{-1}D_x^{\nu}U_\varepsilon(x)+\lambda(x)U_\varepsilon(x)=f(x),\quad x\in(-1,1),\\ &U_\varepsilon(-1)=u_-,\end{aligned}\tag{3.1}$$

where $\lambda(x)$ and $f(x)$ are continuous functions such that $\lambda(x) > 0$ for all $x \in [-1,1]$, $\varepsilon \in (0,1)$ is the singular perturbation parameter and u_- a given constant.

Following the approaches to singularly perturbed Volterra integral and integro-differential equations [11] and the singular perturbed problems of integer order [16, Page 6], we obtain

$$\lambda(x)U_\varepsilon(x) = f(x) + \mathcal{O}(\varepsilon), \quad \varepsilon \to 0,$$

so that if

$$\lim_{x\to -1}\lim_{\varepsilon\to 0} U_\varepsilon(x) \neq \lim_{\varepsilon\to 0}\lim_{x\to -1} U_\varepsilon(x) = u_-,$$

then (3.1) is a singularly perturbed problem with a boundary layer near $x = -1$. We illustrate this situation by a special case with constant functions f and λ.

Proposition 3.1. *If $f(x) = A$ and $\lambda(x) = B$ with $A \in \mathbb{R}$, $B \in \mathbb{R}^+$ for all $x \in (-1,1)$, then the solution of* (3.1) *has the form*

$$U_\varepsilon(x) = \frac{A}{B} + \left(u_- - \frac{A}{B}\right) E_{\nu,1}(-B(x+1)^\nu/\varepsilon), \tag{3.2}$$

where $E_{\alpha,\beta}$ is a two-parameter Mittag-Leffler function defined by

$$E_{\alpha,\beta}(z) := \sum_{k=0}^{\infty} \frac{z^k}{\Gamma(k\alpha+\beta)}, \quad \alpha,\beta > 0. \tag{3.3}$$

Proof. If $\nu \in (0,1)$, then according to Refs. [6,8], we have

$${}_{-1}^{C}D_x^\nu (1+x)^\eta = \begin{cases} \dfrac{\Gamma(\eta+1)}{\Gamma(\eta-\nu+1)}(1+x)^{\eta-\nu}, & \eta > 0, \\ 0, & \eta = 0. \end{cases} \tag{3.4}$$

Since $E_{\nu,1}$ an analytic function, it follows directly from (3.3)-(3.4) that

$${}_{-1}^{C}D_x^\nu E_{\nu,1}\big(-B(x+1)^\nu/\varepsilon\big) = -\frac{B}{\varepsilon} E_{\nu,1}\big(-B(x+1)^\nu/\varepsilon\big),$$

which implies that (3.2) is the solution of (3.1). □

Straightforward calculation shows that

$$\lim_{x\to -1}\lim_{\varepsilon\to 0} U_\varepsilon(x) = \frac{A}{B}, \quad \lim_{\varepsilon\to 0}\lim_{x\to -1} U_\varepsilon(x) = u_-,$$

and the boundary layer appears if $A \neq Bu_-$.

3.2. Petrov-Galerkin schemes

The previous considerations suggest that the collocation method might not provide the results required. As (2.6) shows, the set of the mapped JGL points is very dense in the neighbourhood of $x=-1$ with the distance $\mathcal{O}(N^{-2(l+1)})$ to the nearest interior node. As a result, the matrix of the collocation scheme becomes very ill-conditioned as l increases. Therefore, we prefer to employ a Petrov-Galerkin scheme, where the appropriate choice of testing functions can lead to a diagonal stiffness matrix.

Let us also assume that the term u_- is equal to zero and recall the mappings (2.5) and the notation $\tilde{x}$ — viz.

$$x=-1+2\left(\frac{1+y}{2}\right)^{l+1},\quad y=-1+2\left(\frac{1+x}{2}\right)^{1/(l+1)},\quad \tilde{x}=\left(\frac{1+x}{2}\right)^{1/(l+1)}=\frac{1+y}{2}. \tag{3.5}$$

We denote

$$\Phi_n^{(\nu)}(x):={}_{-1}I_x^{\nu}\,\mathscr{L}_n^{(0,l)}(x),\quad \Psi_n(x):=\mathscr{L}_n^{(0,l)}(x), \tag{3.6}$$

and introduce

$$X_N^{(\nu)}:=\operatorname{span}\{\Phi_n^{(\nu)}\,:\,0\le n\le N\},\quad Y_N:=\operatorname{span}\{\Psi_n\,:\,0\le n\le N\}. \tag{3.7}$$

It follows from the Eqs. (2.27), (2.34) that

$$X_N^{(\nu)}=\operatorname{span}\{(1+x)^{\nu},(1+x)^{\nu+\alpha},\cdots,(1+x)^{\nu+N\alpha}\},\quad Y_N=\mathscr{M}_N^{(0,l)}, \tag{3.8}$$

where $\alpha=1/(l+1)$.

A Petrov-Galerkin spectral scheme for (3.1) with $u_-=0$ is to find $u_N\in X_N^{(\nu)}$ such that

$$\varepsilon\left({}_{-1}^{C}D_x^{\nu}u_N,v_N\right)+(\lambda u_N,v_N)=(f,v_N),\quad v_N\in Y_N. \tag{3.9}$$

We recall that the left-sided Riemann-Liouville fractional derivative of order $\nu\in(0,1)$ are defined by

$$\left({}_{-1}^{R}D_x^{\mu}u\right)(x)=\frac{d}{dx}\left({}_{-1}I_x^{1-\mu}u\right)(x).$$

Using the relations

$${}_{-1}^{R}D_x^{\nu}\,{}_{-1}I_x^{\nu}v(x)=v(x),\quad {}_{-1}^{R}D_x^{\nu}v(x)={}_{-1}^{C}D_x^{\nu}v(x),\quad \text{if}\quad v(-1)=0,$$

presented in [6] and (2.16), we obtain

$$S_{mn}:=\int_{-1}^{1}{}_{-1}^{C}D_x^{\nu}\Phi_n^{(\nu)}(x)\Psi_m(x)dx=\rho_n^{(0,l)}\delta_{mn},\quad \rho_n^{(0,l)}=\frac{2(l+1)}{2n+l+1}. \tag{3.10}$$

Moreover, the Eqs. (2.27), (3.5) yield

$$\Phi_n^{(\nu)}(x)=(1+y)^{(l+1)\nu}Q_n(y),\quad Q_n\in\mathbb{P}_n,$$

so that

$$T_{mn} := \int_{-1}^{1} \lambda(x)\Phi_n^{(\nu)}(x)\Psi_m(x)dx = \frac{l+1}{2^l}\int_{-1}^{1} \lambda(g(y))Q_n(y)P_m^{(0,l)}(y)(1+y)^{l+(l+1)\nu}dy,$$

which can be evaluated by means of the Jacobi-Gauss quadratures with the weight function $(1+y)^{(l+1)\nu}$. The terms

$$f_m := \int_{-1}^{1} f(x)\Psi_m(x)dx = \frac{l+1}{2^l}\int_{-1}^{1} f(g(y))P_m^{(0,l)}(y)(1+y)^l dy$$

can be computed by the Jacobi-Gauss or Legendre-Gauss quadratures.

Representing u_N as $u_N(x) = \sum_{n=0}^{N} \hat{u}_n \Phi_n^{(\nu)}(x)$, one can write the system (3.9) in the matrix form

$$\big(\varepsilon \boldsymbol{S} + \boldsymbol{T}\big)\boldsymbol{u} = \boldsymbol{f}, \tag{3.11}$$

where

$$\boldsymbol{S} = (S_{mn}), \quad \boldsymbol{T} = (T_{mn}), \quad \boldsymbol{f} = (f_0, \cdots, f_N)^t, \quad \boldsymbol{u} = (\hat{u}_0, \cdots, \hat{u}_N)^t.$$

We observe that according to (3.10), the stiffness matrix $\boldsymbol{S}$ is diagonal.

3.3. Numerical results

Example 3.1. We consider the singularly perturbed FIVP (3.1)

$$\varepsilon\, {}_{-1}^{C}D_x^{\nu} U_\varepsilon(x) + U_\varepsilon(x) = 1, \quad x \in (-1,1), \quad \nu \in (0,1); \quad U_\varepsilon(-1) = 0. \tag{3.12}$$

According to (3.2), the solution of (3.12) is

$$U_\varepsilon(x) = 1 - E_{\nu,1}\big(-(x+1)^\nu/\varepsilon\big).$$

It turns out that

$$\lim_{x\to -1}\lim_{\varepsilon\to 0} U_\varepsilon(x) = 1 \neq 0 = \lim_{\varepsilon\to 0}\lim_{x\to -1} U_\varepsilon(x),$$

so $U_\varepsilon(x)$ has a boundary layer at $x=-1$.

We now set $\nu = 0.5$ in (3.9) and apply the Petrov-Galerkin scheme to the corresponding equation. Fig. 3 shows the discrete L^2-norms of $U_\varepsilon - u_N$ against N in log-log scale on the Legendre-Gauss points $\{\xi_i\}_{i=1}^{500}$ for fixed ε or l. In particular, for a fixed ε the increase of the parameter l significantly improves accuracy and convergence rate. On the other hand, smaller ε lead to larger errors. Summarising we note that for thin boundary layers the scheme with $l=3$ or $l=4$ works well. Another advantage of Petrov-Galerkin scheme (3.9) is that it actually incorporates a pre-conditioning technique in the sense of works [19,25]. Thus the Eqs. (3.6)-(3.7) show that the approximate solution is represented via fractional integrals of mapped Jacobi polynomials rather than the mapped polynomials themselves, which leads to a diagonal stiffness matrix. Therefore, the conditioning of the linear system (3.11) does not depend on N but on ε being of order $\mathcal{O}(\varepsilon^{-1})$. Table 2 provides the condition number of the linear system (3.11) for various N and ε.

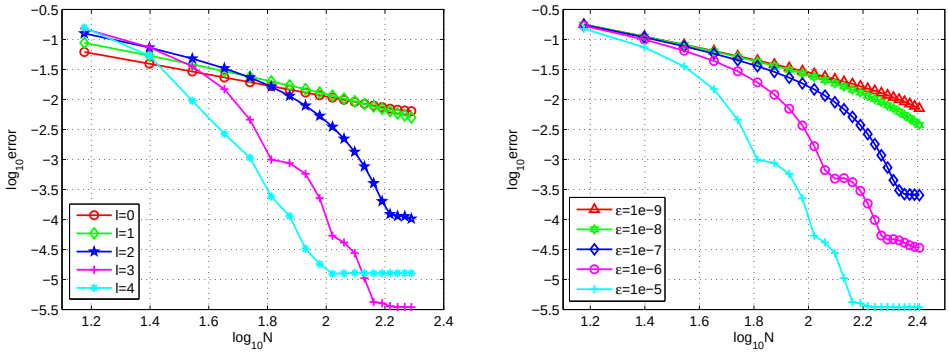

Figure 3: L^2-errors against N in log-log scale. Left: $\varepsilon = 10^{-5}$, l varies; Right: $l = 3$, ε varies.

Table 2: Scaled condition numbers, $\nu = 0.5$, $l = 4$.

N \ ε	10^{-5}	10^{-6}	10^{-7}	10^{-8}	10^{-9}
64	0.9493	0.3319	0.0438	0.0045	0.0004
128	1.1608	1.0845	0.6261	0.1164	0.0127
256	1.1692	1.1666	1.1406	0.9171	0.2941
512	2.1722	2.1819	2.1885	2.2019	2.2167
1024	9.5211	9.5231	9.5232	9.5233	9.5233

Example 3.2. We now consider the Eq. (3.1) with non-constant smooth functions $f(x)$ and $\lambda(x)$. The exact solution of the corresponding equation is not known. Therefore, we compute an approximate solution on a very fine grid and use it as the reference solution to examine the convergence. Thus, let $\nu \in (0,1)$, and consider the equation

$$\begin{aligned} &\varepsilon\, {}_{-1}^{C}D_x^{\nu} U_\varepsilon(x) + (2-x)U_\varepsilon(x) = 2 - \sin x, \quad x \in (-1,1), \\ &U_\varepsilon(-1) = 0. \end{aligned} \tag{3.13}$$

We note that the solution $U_\varepsilon(x)$ has a boundary layer at $x = -1$, since

$$\lim_{x\to -1}\lim_{\varepsilon\to 0} U_\varepsilon(x) = \frac{1}{3}(2+\sin 1) \neq 0 = \lim_{\varepsilon\to 0}\lim_{x\to -1} U_\varepsilon(x).$$

Fig. 4 shows that for $\varepsilon = 10^{-5}$, the use of the corresponding mapping with $l = 4$ substantially diminishes L^2-error. On the other hand, even for the very thin boundary layer of $\varepsilon = 10^{-9}$, the scheme (3.9) with $l = 4$ works reasonably well.

4. Applications to Singularly Perturbed FBVPs

Here we apply mapped spectral Petrov-Galerkin and spectral-Galerkin methods to singularly perturbed Riesz FBVPs of order $\nu \in (1,2)$. Numerical examples demonstrate the efficiency of the schemes.

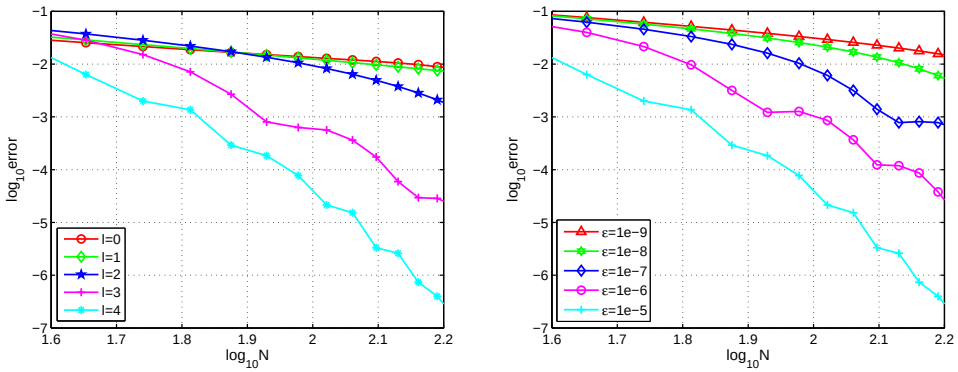

Figure 4: L^2-errors against N. Left: $\varepsilon = 10^{-5}$, l varies. Right: $l = 4$, ε varies.

4.1. Singularly perturbed Riesz FBVPs

Let $\nu \in (1,2)$ and $p, q \geq 0$ are constants such that $p^2+q^2 \neq 0$. We consider the boundary value problem

$$\begin{aligned} &-\varepsilon\, D_x^{\nu} U_\varepsilon(x) + \lambda(x) U_\varepsilon(x) = f(x), \quad x \in (-1,1), \\ &U_\varepsilon(\pm 1) = 0, \end{aligned} \tag{4.1}$$

with the modified Riesz fractional derivative defined by

$$D_x^{\nu} u(x) = \big(p\, {}_{-1}{}^{R}D_x^{\nu} + q\, {}_{x}{}^{R}D_1^{\nu}\big)u(x) = \frac{d^2}{dx^2}\big(p\, {}_{-1}I_x^{2-\nu} + q\, {}_{x}I_1^{2-\nu}\big)u(x).$$

For $p = q = 1$, the operator D_x^{ν} represents the usual fractional Riesz derivative — viz.

$$D_x^{\nu} u(x) = \frac{1}{\Gamma(2-\mu)} \frac{d^2}{dx^2} \int_{-1}^{1} \frac{u(t)}{|x-t|^{\nu-1}} dt, \quad \nu \in (1,2).$$

If

$$\lim_{x \to \pm 1} \frac{f(x)}{\lambda(x)} \neq 0 \quad \text{or} \quad f(\pm 1) \neq 0, \quad \lambda(\pm 1) \neq 0,$$

then the problem (4.1) has boundary layers.

4.2. A spectral-Petrov-Galerkin scheme

We consider the following basis and test functions:

$$\begin{aligned} \widehat{\Phi}_n^{(\nu)}(x) &:= {}_{-1}I_x^{\nu-1}\, \mathscr{L}_n^{(r,l)}(x) + a_n \times {}_{-1}I_x^{\nu-1}\, \mathscr{L}_{n+1}^{(r,l)}(x), \\ \widehat{\Psi}_n(x) &:= {}_{-1}I_x^{1}\, \mathscr{L}_n^{(r,l)}(x) + b_n \times {}_{-1}I_x^{1}\, \mathscr{L}_{n+1}^{(r,l)}(x), \end{aligned}$$

where $\{a_n\}$ and $\{b_n\}$ are so that the boundary conditions $\widehat{\Phi}_n^{(\nu)}(1) = 0$, $\widehat{\Psi}_n(1) = 0$ are satisfied. It is clear that $\widehat{\Phi}_n^{(\nu)}(-1) = 0$, $\widehat{\Psi}_n(-1) = 0$ and we can introduce the solution and test

function spaces

$$\widehat{X}_N^{(\nu)} := \text{span}\big\{\widehat{\Phi}_n^{(\nu)} \,:\, 0 \le n \le N\big\}, \quad \widehat{Y}_N := \text{span}\big\{\widehat{\Psi}_n \,:\, 0 \le n \le N\big\}.$$

The Petrov-Galerkin spectral scheme for the Eq. (4.1) consists in finding $u_N \in \widehat{X}_N^{(\nu)}$ such that

$$\varepsilon\, p\big({}_{-1}^{R}D_x^{\nu-1}\, u_N, v_N'\big) - \varepsilon\, q\big(u_N,\ {}_{-1}^{R}D_x^{\nu}\, v_N\big) + (\lambda u_N, v_N) = (f, v_N), \quad v_N \in \widehat{Y}_N. \tag{4.2}$$

The second term in the left hand side of (4.2) was obtained by the fractional integration by parts. Representing the approximate solution $u_N(x)$ as $u_N(x) = \sum_{n=0}^{N} \tilde{u}_n \widehat{\Phi}_n^{(\nu)}(x)$ and using $\widehat{\Psi}_m(x)$, $m = 0, 1, \cdots, N$ for $v_N(x)$, we write the corresponding system (4.2) in the matrix form

$$\big(\varepsilon p\widehat{\boldsymbol{S}} - \varepsilon q\widehat{\boldsymbol{R}} + \widehat{\boldsymbol{T}}\big)\widehat{\boldsymbol{u}} = \widehat{\boldsymbol{f}}, \tag{4.3}$$

where

$$\widehat{\boldsymbol{S}} = (\widehat{S}_{mn}), \quad \widehat{\boldsymbol{R}} = (\widehat{R}_{mn}), \quad \widehat{\boldsymbol{T}} = (\widehat{T}_{mn}), \quad \widehat{\boldsymbol{f}} = (\widehat{f}_0, \cdots, \widehat{f}_N)^t, \quad \widehat{\boldsymbol{u}} = (\tilde{u}_0, \cdots, \tilde{u}_N)^t,$$

are the matrices with the entries

$$\widehat{S}_{mn} := \int_{-1}^{1} {}_{-1}^{R}D_x^{\nu-1}\, \widehat{\Phi}_n^{(\nu)}(x)\widehat{\Psi}_m'(x)dx, \quad \widehat{R}_{mn} := \int_{-1}^{1} \widehat{\Phi}_n^{(\nu)}(x) {}_{-1}^{R}D_x^{\nu}\, \widehat{\Psi}_m(x)dx,$$
$$\widehat{T}_{mn} := \int_{-1}^{1} \lambda(x)\widehat{\Phi}_n^{(\nu)}(x)\widehat{\Psi}_m(x)dx, \quad \widehat{f}_m := \int_{-1}^{1} f(x)\widehat{\Psi}_m(x)dx.$$

Recalling (2.16) and the properties of fractional derivatives [6] once again, we derive the non-zero entries

$$\widehat{S}_{mn} = \begin{cases} \sigma_{r,l}\gamma_n^{(r,l)} + a_n b_n \sigma_{r,l}\gamma_{n+1}^{(r,l)}, & n = m, \\ b_{n-1}\sigma_{r,l}\gamma_n^{(r,l)}, & n = m+1, \\ a_n \sigma_{r,l}\gamma_{n+1}^{(r,l)}, & n = m-1, \end{cases}$$

of the tridiagonal matrix $\widehat{\boldsymbol{S}}$. On the other hand, both $\widehat{\boldsymbol{R}}$ and $\widehat{\boldsymbol{T}}$ are full matrices. To evaluate them, one can use the Eqs. (2.20)- (2.21) and Jacobi-Gauss quadratures.

4.3. A spectral-Galerkin scheme

The previous scheme generates non-symmetric system. However, if $p = q$, the Galerkin scheme below has symmetric matrices. Thus we seek $u_N \in \widehat{X}_N^{(\nu)}$ such that

$$\varepsilon p\big({}_{-1}^{R}D_x^{\nu-1}\, u_N, Dv_N\big) + \varepsilon q\big(Du_N, {}_{-1}^{R}D_x^{\nu-1}\, v_N\big) + (\lambda u_N, v_N) = (f, v_N), \quad v_N \in \widehat{X}_N^{(\nu)}. \tag{4.4}$$

Representing $u_N(x)$ as $u_N(x) = \sum_{n=0}^{N} \tilde{u}_n \widehat{\Phi}_n^{(\nu)}(x)$ and using $\widehat{\Phi}_m^{(\nu)}(x)$, $m = 0, 1, \cdots, N$ for $v_N(x)$, we write the system (4.4) in the matrix form

$$\big(\varepsilon p\widehat{\boldsymbol{S}} + \varepsilon q\widehat{\boldsymbol{R}} + \widehat{\boldsymbol{T}}\big)\widehat{\boldsymbol{u}} = \widehat{\boldsymbol{f}}, \tag{4.5}$$

where

$$\widehat{\boldsymbol{S}}=(\widehat{S}_{mn}),\quad \widehat{\boldsymbol{R}}=(\widehat{R}_{mn}),\quad \widehat{\boldsymbol{T}}=(\widehat{T}_{mn}),\quad \widehat{\boldsymbol{f}}=(\widehat{f}_0,\cdots,\widehat{f}_N)^t,\quad \widehat{\boldsymbol{u}}=(\tilde{u}_0,\cdots,\tilde{u}_N)^t,$$

are the matrices with the entries

$$\widehat{S}_{mn}:=\int_{-1}^{1}{}_{-1}^{R}D_x^{\nu-1}\,\widehat{\Phi}_n^{(\nu)}(x)D\widehat{\Psi}_m^{(\nu)}(x)dx,\quad \widehat{R}_{mn}:=\int_{-1}^{1}D\widehat{\Phi}_n^{(\nu)}(x)\,{}_{-1}^{R}D_x^{\nu-1}\,\widehat{\Psi}_m^{(\nu)}(x)dx,$$
$$\widehat{T}_{mn}:=\int_{-1}^{1}\lambda(x)\widehat{\Phi}_n^{(\nu)}(x)\widehat{\Psi}_m^{(\nu)}(x)dx,\quad \widehat{f}_m:=\int_{-1}^{1}f(x)\widehat{\Psi}_m^{(\nu)}(x)dx.$$

We note that although $\widehat{\boldsymbol{S}}+\widehat{\boldsymbol{R}}$ is a symmetric matrix since $\widehat{\boldsymbol{S}}=\widehat{\boldsymbol{R}}^T$, all matrices in this scheme are full.

Thus the scheme (4.2) produces a tridiagonal matrix $\widehat{\boldsymbol{S}}$, while the scheme (4.4) generates a symmetric matrix $\widehat{\boldsymbol{S}}+\widehat{\boldsymbol{R}}$. If $p=q$, the schemes (4.2) and (4.4) have almost the same efficiency. However, if $p\neq q$ and $p,q>0$, the matrix $\widehat{\boldsymbol{S}}+\widehat{\boldsymbol{R}}$ for (4.4) is not symmetric anymore, so that the scheme (4.2) looks more attractive.

4.4. Numerical results

Example 4.1. Let $\nu\in(1,2)$ and $p=q=1$. We consider the singularly perturbed Riesz FBVP

$$\begin{aligned}&-\varepsilon\big({}_{-1}^{R}D_x^{\nu}+{}_{x}^{R}D_1^{\nu}\big)U_\varepsilon(x)+(2-x)U_\varepsilon(x)=2-\sin x,\quad x\in(-1,1),\\&U_\varepsilon(\pm1)=0,\end{aligned}$$

and note that since $f(-1)=2+\sin 1\neq 0$, $\lambda(-1)=3\neq 0$, $f(1)=2-\sin 1\neq 0$, $\lambda(1)=1\neq 0$, the solution $U_\varepsilon(x)$ has boundary layers at $x=-1$ and $x=1$.

Fig. 5 demonstrates the errors of the Petrov-Galerkin scheme (4.2) in the cases where ε or r and l are fixed. In particular, we observe that for all r,l and ε, the L^2-error diminishes when N grows. Moreover, the use of mapping technique speeds up the convergence. The results for the Galerkin scheme (4.4) are displayed in Fig. 6. Note that they are similar to the results for the scheme (4.2), but the system of the last scheme has smaller condition numbers — cf. Tables 3 and 4, which leads to smaller round-off errors for larger N.

Example 4.2. Let $\nu\in(1,2)$ and $p=1$, $q=2$. We consider the fractional boundary value problem

$$\begin{aligned}&-\varepsilon\big({}_{-1}^{R}D_x^{\nu}+2\,{}_{x}^{R}D_1^{\nu}\big)U_\varepsilon(x)+(2-x)U_\varepsilon(x)=2-\sin x,\quad x\in(-1,1),\quad \nu\in(1,2),\\&U_\varepsilon(\pm1)=0.\end{aligned}$$

The solution $U_\varepsilon(x)$ has boundary layers again and since $p\neq q$, here we only employ the Petrov-Galerkin scheme (4.2). Fig. 7 shows the decay of errors in L^2-norm and confirms that the mapping technique substantially speeds up the convergence.

Tables 3 and 4 contains scaled condition numbers for two schemes. However, it is more difficult to construct well-conditioned schemes now since the Riesz fractional derivative is, in a sense, a non-symmetric operator.

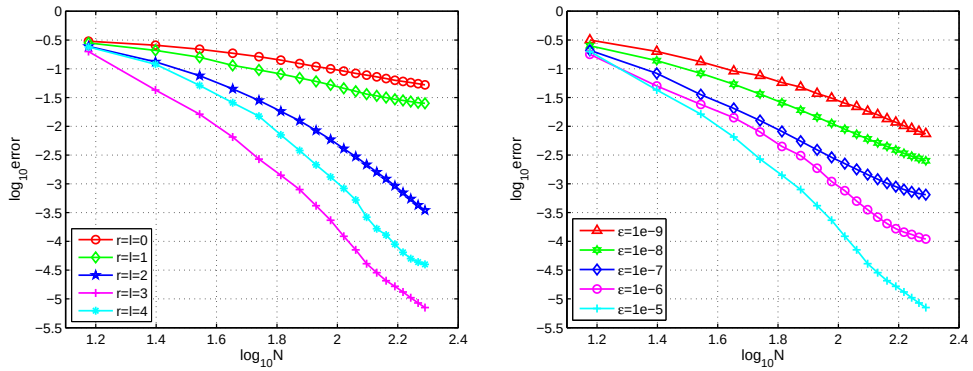

Figure 5: The Petrov-Galerkin scheme (4.2) for Example 4.1: L^2-errors against N in log-log scale, $p=q=1$. Left: $\varepsilon=10^{-5}$. Right: $r=l=3$.

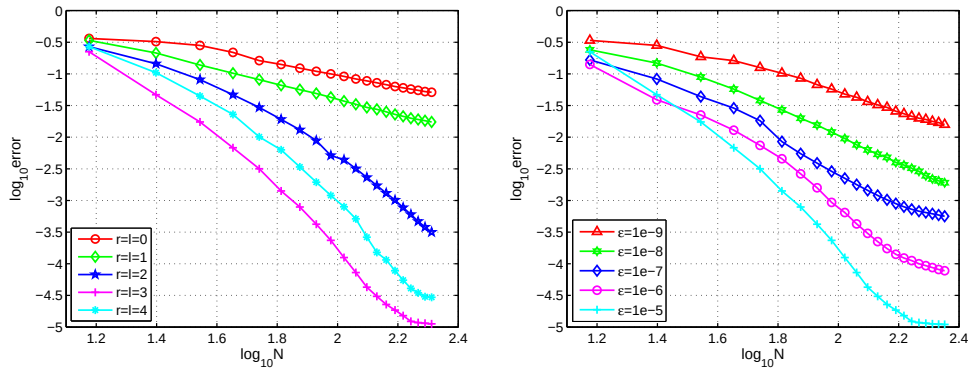

Figure 6: The Galerkin scheme (4.4) for Example 4.1: L^2-errors against N in log-log scale, $p=q=1$. Left: $\varepsilon=10^{-5}$. Right: $r=l=3$.

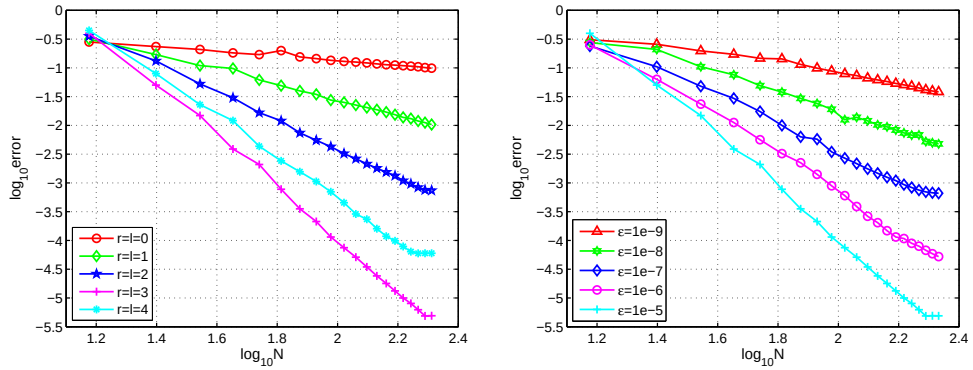

Figure 7: The Petrov-Galerkin scheme (4.2) for Example 4.2: L^2-errors against N in log-log scale with $p=1, q=2$. Left: $\varepsilon=10^{-5}$; Right: $r=l=3$.

Table 3: Scaled condition numbers of (4.3) under different N and ε.

N	$N^{1.8}$	$\varepsilon=10^{-5}$	$\varepsilon=10^{-6}$	$\varepsilon=10^{-7}$	$\varepsilon=10^{-8}$	$\varepsilon=10^{-9}$
64	1782.89	2342.22	2193.44	2107.34	1862.57	1776.83
128	6028.38	6442.72	6253.28	6321.67	6126.58	5998.21
256	21618.82	22034.26	21967.32	21765.35	21603.43	21589.68
512	75281.10	75344.19	75267.24	75316.29	75227.46	75113.94

Table 4: Scaled condition numbers of (4.5) under different N and ε.

N	$N^{2.1}$	$\varepsilon=10^{-5}$	$\varepsilon=10^{-6}$	$\varepsilon=10^{-7}$	$\varepsilon=10^{-8}$	$\varepsilon=10^{-9}$
64	6208.38	7098.34	6847.69	7153.84	6205.04	6387.88
128	26615.89	27962.08	27564.45	27062.61	26364.14	26617.25
256	114104.80	117826.92	116324.66	115948.06	115291.71	114753.48
512	489178.00	491774.69	490341.36	490875.67	489962.93	489453.67

Acknowledgments

The first and second authors would like to thank the Division of Mathematical Sciences at the Nanyang Technological University for hospitality. Part of this work was carried out during their visit to Singapore in 2016.

The research of the first author is supported in part by the NSFC (Grants Nos. 11401380, 11671166, 11701371) and the first level discipline project funding in Statistics subject of Shanghai Lixin University of Accounting and Finance (Grant No. 2017-10), and the third author is partially supported by Singapore MOE AcRF Tier 1 under Grant RG 15/12 and Singapore MOE AcRF Tier 2 under Grants MOE2017-T2-2-014 and MOE2018-T2-1-059.

References

[1] A. Alexandrescu, A. Bueno-Orovio, J.R. Salgueiro and V.M. Pérez-García, *Mapped Chebyshev pseudospectral method for the study of multiple scale phenomena*, Comput. Phys. Commun. **180**, 912–919 (2009).

[2] A. Bayliss and E. Turkel, *Mappings and accuracy for Chebyshev pseudo-spectral approximations*, J. Comput. Phys. **101**, 349–359 (1992).

[3] P. Borwein, T. Erdélyi and J. Zhang, *Müntz systems and orthogonal Müntz-Legendre polynomial*, Comput. Math. Appl. **342**, 523–542 (1994).

[4] C. Canuto, M.Y. Hussaini, A. Quarteroni and T.A. Zang, *Spectral Methods: Fundamentals in Single Domains*, Springer (2006).

[5] E.W. Cheney, *Introduction to Approximation Theory*, AMS Chelsea Publishing (1998).

[6] K. Diethelm, *The Analysis of Fractional Differential Equations*, Lecture Notes in Mathematics **2004**, Springer (2010).

[7] S. Esmaeili, M. Shamsi and Y. Luchko, *Numerical solution of fractional differential equations with a collocation method based on Müntz poynomials*, Comput. Math. Appl. **62**, 918–929 (2011).

[8] R. Gorenflo, A.A. Kilbas, F. Mainardi and S.V. Rogosin, *Mittag-Leffler Functions, Related Topics and Applications Theory and Application*, Springer (2014).
[9] D. Gottlieb and S. Orszag, *Numerical Analysis of Spectral Methods: Theory and Applications*, SIAM (1977).
[10] D.M. Hou and C.J. Xu, *A fractional spectral method with applications to some singular problems*, Adv. Comput. Math. **43**, 911–944 (2017).
[11] J.P. Kauthen, *A survey of singularly perturbed Volterra equations*, Appl. Numer. Math. **24**, 95–114 (1997).
[12] D. Kosloff and H. Tal-Ezer, *A modified Chebyshev pseudospectral method with an $O(N^{-1})$ time step restriction*, J. Comput. Phys. **104**, 457–469, 1993.
[13] W.B. Liu and J. Shen, *A new efficient spectral Galerkin method for singular perturbation problems*, J. Sci. Comput. **11**, 411–437 (1996).
[14] W.B. Liu and T. Tang, *Error analysis for a Galerkin-spectral method with coordinate transformation for solving singularly perturbed problems*, Appl. Numer. Math. **38**, 315–345 (2001).
[15] P.C. McCarthy, J.E. Sayre and B.L.R. Shawyer, *Generalized Legendre polynomials*, J. Math. Anal. Appl. **177**, 530–537 (1993).
[16] J.J.H. Miller, E. O'Riordan and G.I. Shishkin, *Fitted Numerical Methods for Singular Perturbation Problems*, World Scientific (2012).
[17] G.V. Milovanović, *Müntz orthogonal polynomials and their numerical evaluation*, in: *Applications and Computation of Orthogonal Polynomials*, W. Gautschi, G. Opfer and G.H. Golub (Eds), pp. 179–194, Birkhäuser (1999).
[18] I. Podlubny, *Fractional Differential Equations: An introduction to fractional derivatives, fractional differential equations, to methods of their solution and some of their applications*, Mathematics in Science and Engineering **198**, Academic Press Inc. (1999).
[19] J. Shen, *Efficient spectral-Galerkin method. I. Direct solvers of second- and fourth-order equations using Legendre polynomials*, SIAM J. Sci. Comput. **15**, 1489–1505 (1994).
[20] J. Shen and L.L. Wang, *Error analysis for mapped Legendre spectral and pseudospectral methods*, SIAM J. Numer. Anal. **42**, 326–349 (2004).
[21] J. Shen, T. Tang and L.L. Wang, *Spectral Methods: Algorithms, Analysis and Applications*, **41** of *Series in Computational Mathematics*, Springer-Verlag (2011).
[22] J. Shen and Y. Wang, *Müntz-Galerkin methods and applications to mixed Dirichlet-Neumann boundary value problems*, SIAM J. Sci. Comput. **38**, A2357–A2381 (2016).
[23] G. Szegö, *Orthogonal Polynomials (Fourth Edition)*, AMS Coll. Publ. (1975).
[24] T. Tang and M.R. Trummer, *Boundary layer resolving pseudospectral methods for singular perturbation problems*, SIAM J. Sci. Comput. **17**, 430-438 (1996).
[25] L.L. Wang, M. Samson and X.D. Zhao, *A well-conditioned collocation method using pseudospectral integration matrix*, SIAM J. Sci. Comput. **36**, A907–A929 (2014).
[26] L.L. Wang and J. Shen, *Error analysis for mapped Jacobi spectral methods*, J. Sci. Comput. **24**, 183–218 (2005).